On the Use of Close-Range Digital Stereo-Photogrammetry to Measure Gravel-Bed Topography in a Laboratory Environment

Stephane Bertin
PhD Student, Dept. of Civil and Environmental Engineering, Auckland Univ., Auckland 1010, New Zealand. Email: sber081@aucklanduni.ac.nz

Heide Friedrich
Lecturer, Dept. of Civil and Environmental Engineering, Auckland Univ., Auckland 1010, New Zealand. Email: h.friedrich@auckland.ac.nz

Patrice Delmas
Senior Lecturer, Dept. of Computer Science, Auckland Univ., Auckland 1010, New Zealand. Email: p.delmas@auckland.ac.nz

Edwin Chan
PhD Student, Dept. of Computer Science, Auckland Univ., Auckland 1010, New Zealand. Email: ycha171@auckland.ac.nz

ABSTRACT: There is a need for high-resolution topographical data of riverine gravel-beds for hydraulic studies. To date, there is no readily affordable and deployable technique to collect these data, especially over submerged topographies. Terrestrial laser-scanners and proprietary stereo-photogrammetric systems, with associated commercial software, allow exposed gravel-beds to be represented as high-resolution Digital Elevation Models (DEMs), both in the laboratory and in the field. Some measurements, yet sparse, were obtained through-water. However, either the necessary equipment (hardware/software) or the complexity of the methodology restrained the applicability of the findings. For stereo-photogrammetry to be used in hydraulic research, the promise of a versatile technique, which can be adapted to varied experiments, with quick high-resolution data acquisition, warranted further development. In this paper, a low-cost stereo-photogrammetric system, and its application for gravel-bed studies, is presented, together with an internal performance evaluation. The setup and its principle of operation, which make use of digital consumer cameras and non-commercial photogrammetric process steps, differ from previous photogrammetric systems employed for gravel-bed morphology characterization. The developed system is used in laboratory experiments measuring a water-worked gravel-bed made of fine sediment particles (D_{50} of 7-mm). A variety of DEMs with 0.5-mm ground resolution, obtained over the same gravel-bed with variable surface coverage and water depth, is presented and the extracted metrics are compared. The presented photogrammetric system shows promise in the advent of a new method for gravel-bed topography measurement at the grain-scale, which allows data to be obtained with minimum disturbance.

KEY WORDS: Remote sensing, Stereo-photogrammetry, Gravel-bed, DEM, Roughness, Image processing.

1 INTRODUCTION

Advances in Fluid Mechanics and Hydraulics are intimately connected to technological progress and the development of new methods (USNCTAM, 2006). Studies, such as turbulence and flow resistance research, have been made possible by the measure of fine quantities of velocity fields and their variations in space and time. In environmental flows, such as in alluvial rivers, the water flow pattern is strongly influenced by the flow boundaries. In response, water-worked surfaces generally present a complex arrangement with both a spatial and a temporal dependence (Nikora et al., 1998, Mao et al., 2011). Measuring topography in riverine environment has enabled numerous studies (roughness characterization, river channel evolution, erosion and deposition, scouring process) and provided models to be used in numerical simulations of flow over rough surfaces.

Gravel-bed rivers represent a difficult environment for topography measurement. Generally, in-situ measurement, with as little disturbance as possible of the medium under investigation, is preferred. More

specifically, there is a need for high-resolution topographical data, which enable sediment particle representation and interstices between them (Smart et al., 2004). This allows giving critical insights on mechanisms such as those responsible for the development of gravel-bed surfaces, but also for grain-resistance to the flow and sediment entrainment (Hodge et al., 2008, Mao et al., 2011).

During the 1990s, available techniques, like physical profilers made of measuring rods, only enabled longitudinal profiles to be obtained, with coarse measurement density and long measuring time. Obtained results motivated the quest of more advanced techniques. The use of terrestrial laser-scanners (TLSs) and stereo cameras started on exposed gravel-beds. High-resolution DEMs were obtained in the laboratory and in the field (Butler et al., 2001, Smart et al., 2004, Hodge et al., 2008). However, close-range measurement of submerged topography using TLSs and photogrammetric systems has been limited to very few studies (Butler et al., 2002, Smith et al., 2012). In general, the former technique can generally be described as more precise, ready-to-use, but more expensive and less versatile. On the other hand, cameras have become important instruments in Fluid Mechanics laboratories, with varied applications. Associated with computer vision and image processing techniques, 3D models can be extracted from stereo photographs. This served to measure riverine environment at different spatial scales. Westaway et al. (2001) utilized aerial photographs to measure the morphology of clear-water, shallow, gravel-bed rivers with areal coverage of the order of several hundred meters along the main axis and pixel size in the object space less than 0.1-m. Butler et al. (2002) measured through-water the organization of gravel particles, both in the laboratory and in the field, with ground resolution DEMs of 3-mm. However, special cameras and commercial photogrammetric software were utilized, which imposed the type of calibration. The exterior orientation of the cameras, necessary for stereo reconstruction, was computed after the location of photo-controlled targets disposed on the riverbed was measured with total stations. This restrained the applicability of the technique. In Chandler et al. (2001) and Rapp et al. (2012), photogrammetric systems made of digital consumer cameras were developed and applied to hydraulic measurements. In Bertin et al. (2011, 2012), Chan et al. (2012) and Bouratsis et al. (2013), a different calibration method and non-commercial photogrammetric process steps were added to the digital cameras to produce new and low-cost photogrammetric setups. However, since Butler et al. (2002), no high-resolution photogrammetric measurement of submerged gravel-beds has been published.

2 DESCRIPTION OF THE TEST

Topographic data were obtained with stereo-photogrammetry over the same armored gravel-bed, under varied conditions. Two measurement windows, 450 x 400-mm in the flow and transverse direction, respectively, and 850 x 400-mm, hereafter referred to as the *small* and the *large* measurement window, were utilized for in-air measurement. Through-water measurement was undertaken over the small measurement window with four different water depths: 40-mm, 100-mm, 150-mm and 200-mm, covering the range of water depths generally used in laboratory experiments on gravel-beds. At total, six datasets hereafter referred to as the six *measurement scenarios* were obtained on the same gravel-bed. To clarify the name given to the measurement scenarios, *through-water* measurement hereafter refers to cameras placed above the water surface, viewing the gravel-bed underwater (submerged), while *in-air* measurement refers to the traditional case of cameras in air viewing the gravel-bed in air (exposed).

Topography measurement was undertaken over a water-worked gravel-bed (in contrast to a man-made screeded bed) to assess photogrammetric capabilities in measuring grains' arrangement on natural riverine surfaces. The simulated gravel-bed was prepared in a 19-m long sediment-starved tilting flume, with dimensions 0.45-m wide and 0.5-m deep. The slope of the flume bed was set to 0.5%. Photogrammetric measurements were obtained on a vertically adjustable test section, located 10-m downstream of the flume inlet, comprising of a fixed bed with a 950-mm long and 450-mm wide recess. The recess, surrounded by a fixed bed artificially roughened, was filled with graded and rounded natural riverine sediment. The properties of the prepared mixture are 0.7-mm<d<55-mm, a D_{50} of 7-mm, and a geometric standard deviation of the sediment distribution, calculated as $\sqrt{D_{84}/D_{16}}$, of 3.16 (Figure 1). Initially, a screeded bed was created by placing the sediment into the base of the recess. The surface was flattened to a thickness of 100-mm, at the same height than the surrounding bed. The sediment bed was water-worked for 44-hours at a constant flow rate Q = 62-L/s, monitored by a pre-calibrated orifice gauge in the flume's feeding pipe, and a freely adjusted water depth of 170-mm. A uniform flow was obtained

along the length of the flume. A 200-mm long, full-width, shallow sediment trap, located 400-mm downstream of the test section, enabled the collection of the eroded sediment. The experiment was halted after two consecutive hours of no-sediment collected in the trap, whilst it was considered a static armor layer had formed on the gravel-bed surface.

For each measurement scenario, data collection consisted in the acquisition of three sets of images, simultaneously with the two cameras: 30 calibration images, 10 'rectification-check' images and 5 images of the gravel-bed. This required a calibration above the armored gravel-bed. A flat plate, the size of the sediment recess, was placed a few centimeters above the fragile gravel-bed to act as a cover during the calibration. This raised a problem in the case of 40-mm water depth. The distance between the gravel-bed cover and the water surface was too small to move the calibration pattern in between, and in-air calibration was performed instead of through-water. The water depths under investigation were adjusted by moving a sharp-edge weir at the end of the flume. A ruler, with zero-mark corresponding to the elevation of the initial screeded bed surface, was utilized to check that the water depth was adequate. The water depths were maintained constant throughout the acquisition of the three sets of images constituting the photogrammetric data. The flow rate was reduced significantly to obtain good photographs through-water, until a nearly flat water surface was achieved. Flow rates of up to 7-L/s were found suitable for the water depths considered and obviated the need of a Perspex sheet to flatten the water surface. The flume was finally drained and dried during two days to allow in-air photogrammetric measurement. After data were collected in the laboratory, data processing was undertaken in the office using an Alienware laptop with Intel core CPU @ 2.20GHz, 8GB memory, and MATLAB R2010b.

3 GRAVEL-BED MEASUREMENT WITH STEREO-PHOTOGRAMMETRY

3.1 A low-cost consumer-grade stereo-photogrammetric system

The system developed for this study comprises two Nikon D90 digital consumer cameras, with a 20-mm lens and a 5.5-µm pixel pitch (12.3-megapixel). The two cameras are rigidly attached at the horizontal above the test section in canonical configuration (with parallel optical axis), on a frame sliding along the flume (Figure 1). The distance between the cameras and the gravel-bed is adjustable within the range of 0.5-m to 1.5-m. The baseline (i.e. the horizontal distance between the cameras) can be adjusted from 200-mm to 400-mm. Each camera is connected to a computer, enabling live view and remote control. The settings for both cameras are manually adjusted to be identical (F/22 aperture, ISO 200, 5000K color temperature) and manually focused on the gravel-bed. A shutter speed of 1/3-s was used for images of the gravel-bed and 1/10-s for images of the calibration pattern.

The lighting environment is set up with four 1-m neon lights positioned on the two transparent sides of the flume, with two neon lights on each side, one above the other. Thin white Plexiglas layers are applied against the flume's glass walls. They act as a light diffuser and allow obtaining a homogenous lighting of the gravel-bed with little reflection on the stones. In a previous study, light reflection at the grains' surface was found detrimental on DEM quality (Bertin et al., 2011).

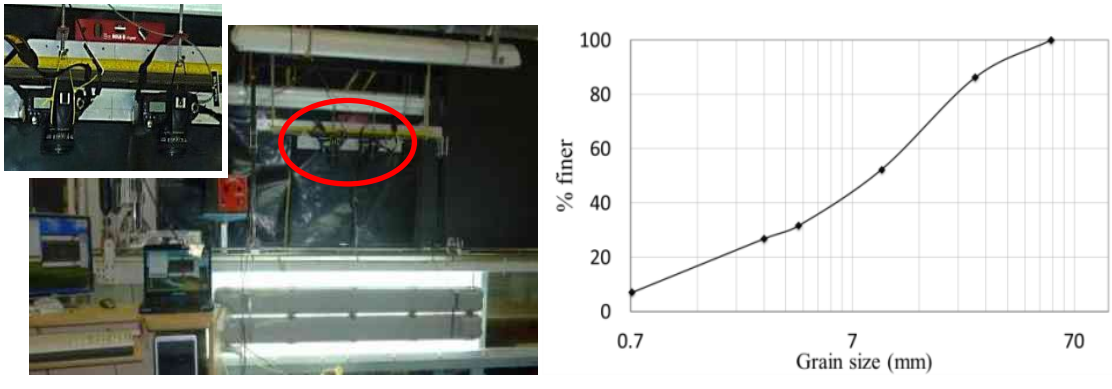

Figure 1 The photogrammetric setup (left) and particle size distribution from size sieving (right).

3.2 The photogrammetric process steps

This section presents all important practical information on the photogrammetric process steps utilized in the study to reconstruct DEMs of the gravel-bed from stereo photographs and make an internal evaluation of the performance. It was chosen to present each photogrammetric process step in a separate table. Theoretical descriptions of the photogrammetric process steps can be found in the cited references.

Design of optimum setup and definition of its capabilities

Objective	Set the height of the cameras above the mean level of the gravel-bed to suit the experimental requirements and get the best measurement specifications.
Inputs	Cameras' parameters (focal length, sensor dimensions, pixel size), baseline, water depth (if any), margin dimension, range of bed elevations around zero-mean bed level and size of the measurement window.
Method	A compiled MATLAB program makes use of standard photogrammetric equations and the Snell-Descartes law of Optics to compute the minimum height of the cameras to cover the measurement window (*ideal height*) and the resulting photogrammetric parameters (Table 1).
In practice	- The baseline (i.e. distance between the two cameras) was set to 250-mm for the small measurement window and 300-mm for the large measurement window, to limit the risk of occlusions in the depth map, where regions are seen by one camera only. - The range of disparity, associated with the extreme elevations of the gravel-bed, was computed by pre-supposing a range of gravel-bed elevations of 50-mm centered on the mean-bed level. - Streaks are often present near the edges of the depth map (also seen in Butler et al. (2002)). A margin of 50-mm around the desired test section was accounted in the design and cropped before analysis. - Using a measuring rod and a tape ruler, the height of the cameras above the mean bed level and the baseline can be set with an expected precision of ±10-mm and ±1-mm, respectively. As such, the actual photogrammetric parameters may differ slightly from the parameters determined for the ideal cameras' height. Because of this, all parameters calculated are rounded to the nearest value.

Table 1 Summary of the setups designed for the test. All values are given in millimeter, except the range of disparity (pixel), the overlap between the two images (%) and the number of pixels (-).

	Setup 1	**Setup 2**	**Setup 3**	**Setup 4**	**Setup 5**	**Setup 6**
Water depth	0	40	100	150	200	0
Calibration	In-air	In-air	Through-water	Through-water	Through-water	In-air
Rounded ideal height	679	691	709	724	739	1060
CFoV[1]	550 x 531	550 x 532	550 x 533	550 x 534	550 x 535	950 x 830
Baseline	250					300
Range of disparity	[1292 1391]					[1005 1054]
Overlap	69					76
Measurement spacing / resolution	0.19 29-pixel/mm^2					0.29 12-pixel/mm^2
Depth accuracy	0.5					1.0
Measurement window	450 x 400					850 x 400
Number of pixels in measurement window	5,200,000					4,000,000^L 2,100,000^S

[1]Size of Common Field of View (CFoV) between the two cameras, where 3D measurement is possible; [L]Number of pixels over 850 x 400-mm; [S]Number of pixels over 450 x 400-mm.

Mechanical alignment of the stereo rig

Objective	Minimize the necessary correction, called stereo rectification, applied to images before stereo matching.
Method	- The cameras are put above the gravel-bed with the arrangement determined during the design. - A large checkerboard is placed above the gravel-bed. Tights and shims help adjust the orientation of each camera until a good alignment (i.e. corners of the checkerboard situated on the 'same scan line' in the left and in the right image) is verified by eye using computer live view.

Calibration of the stereo-photogrammetric setup and image stereo rectification

Objective	Compute cameras' intrinsic and extrinsic parameters to allow image stereo rectification.
Inputs	30 stereo images of the calibration pattern (called *checkerboard*) in different orientations (using all degrees of freedom), carefully covering the measurement window.
Method	Bouguet's calibration toolbox for MATLAB, freely available on Bouguet's webpage (http://www.vision.caltech.edu/bouguetj/calib_doc/), where Zhang calibration (Zhang (1998)) and image stereo rectification using the technique of Fusiello et al. (2000) are implemented.
In practice	- Checkerboard orientated manually for in-air calibration; orientated using blocks and wedges underneath for through-water calibration. - A short shutter speed of 1/10-s reduced the risk of shaking/blur in the photographs - Interval timer shooting of 7-s was enough to orientate the checkerboard and freeze the position for in-air calibration. - Interval timer shooting of 40-s in case of through-water calibration so that the free surface waves, which formed when the checkerboard was moved from a position to another, were sufficiently diminished to obtain good photographs through-water (see Figure 2). - Calibration done in-situ, at the location where the riverbed is measured, to avoid moving the setup and prevent changes in cameras' positioning. - Independent calibration sets made the more similar possible to minimize the differences in results between the measurement scenarios due to different calibration images. - Checkerboard printed on A4 sheets, and matte laminating in the case of through-water calibration, glued on flat Perspex. 30-mm square size allowed good automatic corner recognition at the distances considered. - The presented test differs from a 'standard experiment' where one arrangement of the cameras is generally utilized. For the latter, it is recommended that the calibration process is undertaken prior the experiment starts not to disturb any water-worked gravel-bed and that the cameras are leaved untouched for the whole duration of the experiment.

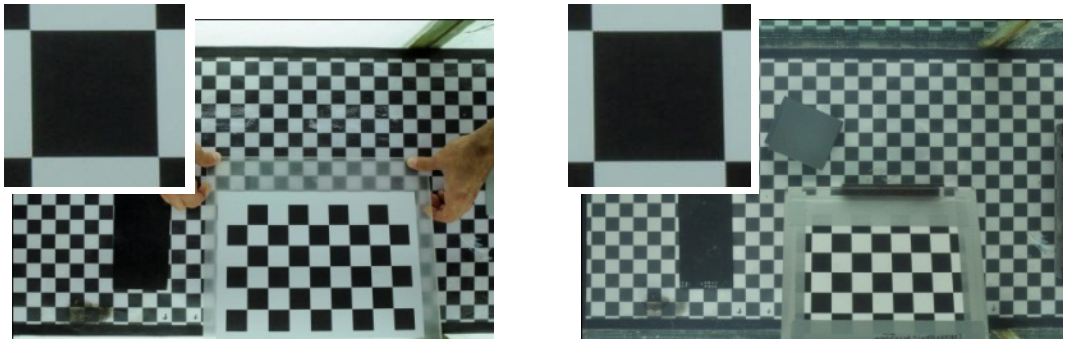

Figure 2 Left-camera image of the checkerboard obtained in air with setup 1 (left) and with 200-mm water depth with setup 5 (right) with a zoom on the red-squared corner. In the background is the large checkerboard used for mechanical alignment, which also protected the gravel-bed during the calibration.

Image rectification assessment

Objective	Evaluate the accuracy of the rectification process.
Inputs	An additional set of 10 images of the checkerboard under different positions. This set of images, called the 'rectification-check', was obtained in the same conditions as the calibration images.
Method	The rectification-check images are stereo rectified using the calibration results. A compiled MATLAB program compares the vertical location of the four extreme corners of the checkerboard between the left and right rectified images (Table 2).
Remarks	- Rather than gluing sharp objects on the gravel-bed, which could disturb it, it is preferred to measure the rectification error through an independent set of calibration images. - In epipolar configuration, a point will ideally be found on the same scan line in the left and the right image constituting a stereo pair.

	- Bouguet's calibration toolbox gives clues on the accuracy of the calibration results via the uncertainties on the calibration parameters and the pixel error between estimated and measured corners of the checkerboard, called reprojection error (see Table 2). However, this does not indicate if the image stereo rectification is correctly executed.

Stereo matching of corresponding pixels

Objective	Produce 3D images the size of the CFoV, called depth maps or disparity maps.
Inputs	- 5 RGB stereo images of the gravel-bed after stereo rectification (Bouguet's function for stereo rectification was modified to obtain not only grey-scale rectified images). - Disparity search range computed during the design of the stereo rig.
Method	The Symmetric Dynamic Programming Stereo (SDPS) algorithm, developed by researchers at the University of Auckland, matches corresponding pixels in the 5 stereo images to produce 5 depth maps.
Remarks	- Stereo matching is governed by pixels' stereo correspondence, which is the similarity of optical signals between the left and the right image in a stereo pair (Gimel'farb, 2002). - Color images, generally offering more variations in signal intensity than grey-scale images, were used for stereo matching. - Various parameters can be adjusted in the SDPS, like the color adaptation factor, the occlusion penalty weight and the visual smoothing of the depth map. For the presented test, all parameters were kept to the default values.

Point cloud extraction

Objective	The 3D coordinates of all pixels contained in a depth map are extracted and saved in a text file.
Inputs	- 5 depth maps of the gravel-bed. - Calibration results.
Method	A compiled program in C++ extracts the metrics behind the 5 depth maps to create 5 point clouds.
Remarks	- The point clouds in our test contained the 3D coordinates of several million pixels (measured points) and were about 250-MB. - The measured points are non-regularly distributed inside a point cloud, because they are related to different depths, and pixel size is depth-dependent.

ANOVA test on stereo matching

Objective	Analysis of variance in the 5 point clouds available for each measurement scenario (Table 3).
Method	Differentiate the point clouds in MATLAB to compute Repeat Scan Error Values (RSEV) of bed elevations over the small and the large measurement window, with setup 1 to 5 and setup 6, respectively.
Remarks	The 5 stereo pairs available for each measurement are obtained in a row and stereo rectified using the same calibration results. The rectification error is thus identical in all stereo pairs. Differences between the obtained point clouds are thought to result from the neon lights, which pulse stripes of lights non-uniformly in time, creating varying stereo correspondence in the stereo pairs. Correct synchronization of the cameras is thus important, and was done with care, although manually.

DEM reconstruction

Objective	Average 5 point clouds to produce one DEM.
Method	- The point clouds are directly opened with MATLAB and interpolated on a regular grid with 0.5-mm spacing, using the function "Gridfit", the triangle interpolation method and a smoothing setting of three. - The resulting matrices are merged to produce one matrix of bed elevations. - The final DEM is normalized to get a zero-mean bed level and rotated to get the x-axis orientated in the flow direction.
Remarks	After preliminary tests, it was found that a smoothing setting of 3 improved the shape of the particles, reducing the 'staircase' aspect, which is present in point cloud data due to stereo-vision limitation of depth resolution (Figure 3).

3.3 Analysis and comparison of surface elevations

To obtain a comparison between the different measurement scenarios, all DEMs were detrended. In Smart et al. (2004), bed-elevation data, obtained with a laser-scanner and a physical profiler, were detrended with a surface trend created after bi-cubic spline interpolation of grid points elevation. In our study, a bi-quadratic filter was utilized, as this reduced the variance of the original data the most, similar to Goring et al. (1999). The difference in variance between the original surface and the detrended surface is in the order of the square measurement accuracy.

The DEM obtained with setup 6, over the large measurement window, was first reduced to the size of the small measurement window before being detrended (hence with a surface trend measured over the small measurement window, to be directly comparable with the other setups).

Detrending, prepares the data for subsequent work on roughness characterization (Nikora et al., 1998, Goring et al., 1999, Smart et al., 2004), as it removes any difference in orientation between the setups. After detrending, the DEMs are identically aligned along the vertical. They can be differentiated and the extracted metrics from each DEM can be compared (see Table 4)

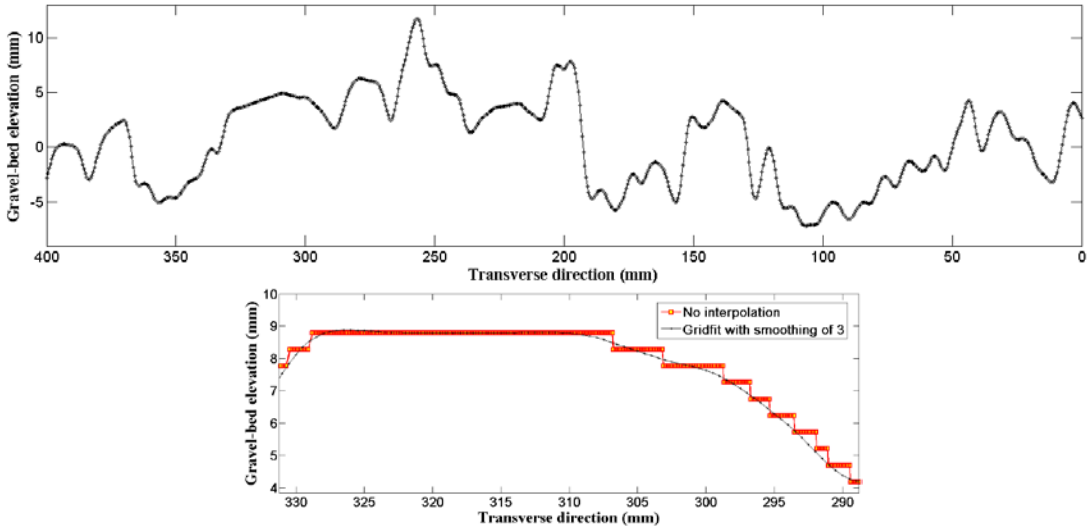

Figure 3 Profile of detrended bed elevations along the transverse direction to the flow obtained with setup 1, downstream direction = 160-mm, as marked in Figure 4 (top). The 'staircase' aspect is shown in detail for a top of a larger gravel particle, comparing point cloud data on non-uniform grid, with the DEM data on uniform grid (bottom).

4 RESULTS

4.1 Effect of water depth on photogrammetric measurements

Although the reprojection error (Table 2) tends to show that the accuracy of the calibration remains high for each setup, the rectification error (both mean and standard deviation) increases with increasing water depth. In Bertin et al. (2012), it was suggested that a sub-pixel rectification error is important to minimize the risk of mismatched pixels during stereo matching. As seen in Table 2, all setups verify this requirement except setup 5 (200-mm water depth).

RSEV also increase in average with increasing water depth (Table 3). The minimum RSEV was obtained with setup 1 (450 x 400-mm in-air measurement). Setup 5 does not present any RSEV larger than 5-mm, despite the largest mean RSEV in absolute of 0.1799-mm. The proportion of RSEV larger than 5-mm in setups 2, 3, 4 and 6 is very small, especially when compared with RSEV associated with repeated laser-scans over patches of exposed gravel-beds in the field (Hodge et al., 2008), where RSEV larger than a threshold (ranging between 2 and 12-mm) represented more than 20% of the initial number of points. It means that stereo matching is robust and random errors are rare.

Figure 4 presents the detrended DEMs of bed-surface elevations obtained over the small and the large measurement window with setups 1 to 6. In-air measurement (setup 1) served as a ground truth for comparison, not because of the better vertical accuracy but because additional errors generally result from

through-water measurement (Butler et al., 2002, Smith et al., 2012). The DEMs show that all setups were able to measure the main features present on the gravel-bed surface. The only obvious measurement errors distinguishable on the DEMs are found in the top left corner of the DEM obtained with setup 2 (40-mm water depth) and at the same location but to a lesser extent with setups 4 and 5. DEMs provide an efficient way to visually check, but not to compare the obtained metrics. Statistics presented in Table 4 and PDFs presented in Figure 5 however enable that. The large range of bed elevations observed with setup 2 shows that obvious measurement errors happened when the gravel-bed was measured with 40-mm water depth. These large errors are however located near the edges of the DEM. Setup 3 (100-mm of water depth) enabled the gravel-bed to be measured in a very similar way as the exposed gravel-bed.

Table 2 Summary of reprojection and rectification errors.

	Setup 1	**Setup 2**	**Setup 3**	**Setup 4**	**Setup 5**	**Setup 6**
Mean reprojection error in absolute (pixel)	$0.0156^{L,x}$ $0.0115^{L,y}$ $0.0208^{R,x}$ $0.0215^{R,y}$	*NA*	$0.0143^{L,x}$ $0.0153^{L,y}$ $0.0257^{R,x}$ $0.0355^{R,y}$	$0.0147^{L,x}$ $0.0161^{L,y}$ $0.0186^{R,x}$ $0.0150^{R,y}$	$0.0186^{L,x}$ $0.0176^{L,y}$ $0.0193^{R,x}$ $0.0206^{R,y}$	$0.0124^{L,x}$ $0.0130^{L,y}$ $0.0219^{R,x}$ $0.0197^{R,y}$
Rectification error (pixel)	0.3959^{M} 0.1293^{S}		0.2840^{M} 0.1647^{S}	0.5626^{M} 0.2223^{S}	1.0851^{M} 0.4119^{S}	0.4276^{M} 0.0396^{S}

^{L}Left camera; ^{R}Right camera; ^{x}Horizontal direction in photograph; ^{y}Vertical direction in photograph; ^{NA}Not available since calibration and rectification-check images were obtained and processed in air, and are thus not representative of the real reprojection/rectification error underwater; ^{M}Mean in absolute; ^{S}Standard deviation in absolute.

Table 3 Repeat Scan Error Values (RSEV).

Setup 1	**Setup 2**	**Setup 3**	**Setup 4**	**Setup 5**	**Setup 6**
0.0843^{M}	0.1062^{M}	0.1434^{M}	0.1720^{M}	0.1799^{M}	0.1537^{M}
0.0027^{S}	0.0292^{S}	0.0143^{S}	0.0120^{S}	0.0035^{S}	0.0888^{S}
0^{P}	0.0248^{P}	0.0046^{P}	0.0122^{P}	0^{P}	0.0098^{P}

^{M}Mean in absolute (mm); ^{S}Standard deviation in absolute (mm); ^{P}Maximum percentage of RSEV > 5-mm (%).

Overall, the Z_{MIN} values (the lowest troughs on the gravel-bed surface) are reduced in absolute with increasing water depth (Table 4). It can be inferred that through-water measurement tends to prevent the correct characterization of the troughs in the gravel-bed, especially with a water depth of 200-mm. The Z_{MAX} values (highest peaks) are increased with increasing water depth, which means that spikes tend to be more frequent. These spikes however represent a very small proportion of the ensemble of elevations, as seen with the PDFs.

The standard deviation of detrended bed elevations σ_Z has been shown to relate well with the vertical roughness length in relatively rough flow resistance equations (Smart et al., 2004). It is thus interesting to see what happens to this parameter when through-water measurement is undertaken (Table 4). The σ_Z obtained over the submerged beds with 100-mm and 150-mm water depth are identical to the σ_Z value obtained over the exposed gravel-bed. The standard deviation only reduces slightly with 200-mm water depth. When the gravel-bed submerged with 40-mm of water was measured, the standard deviation in bed elevations was seriously reduced, which means that roughness statistics extracted from this model would not be representative.

After detrending with a bi-quadratic filter and (manual) horizontal alignment of the DEMs, DEMs obtained with setups 2 to 6 were differentiated with the DEM obtained with setup 1. Contour plots were obtained as well as PDFs of the difference in surface elevations. These plots, which are not presented here, give more insights on where the errors happen in the case of through-water measurement. It can be seen that most errors are located near the edges of the measurement window. This stresses the importance of adding a margin around the desired test section to obtain good topographic data through-water. The same conclusion was drawn when RSEV were computed over the CFoV. Indeed, RSEV in the 50-mm margin around the measurement window are significantly larger (with a minimum of a two-fold increase) compared to RSEV inside the measurement window.

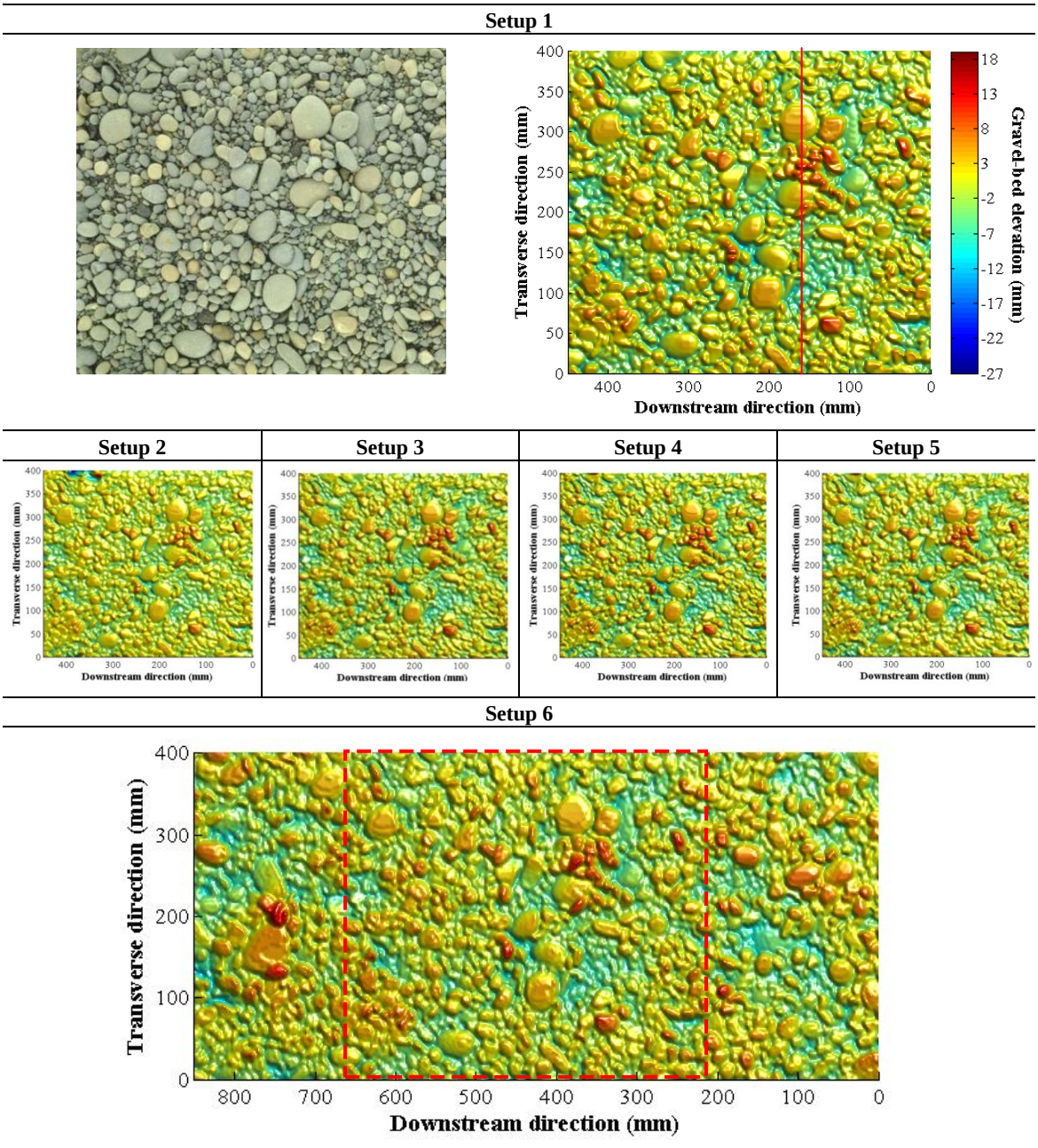

Figure 4 Photograph of the small measurement window and detrended DEMs obtained with setups 1 to 6. The same color mapping was applied to all DEMs to facilitate the visual comparison. The red line in the DEM of setup 1 shows the location of the transverse profile as seen in Figure 3.

4.2 Effect of areal coverage

When cameras were elevated higher away from the gravel-bed, to cover the large measurement window, this was accompanied by a coarser measurement resolution (12-pixel/mm^2 instead of 29-pixel/mm^2) and deteriorated accuracy (1.0-mm instead of 0.5-mm) (see Table 1). The PDF of bed surface elevations for setup 6 was calculated over the original large-scale DEM cropped to the size of the small measurement window to enable comparison with the other PDFs (Figure 5). The change in measurement resolution between setup 1 and setup 6 does not affect the representation of particles' shape and the interstices between them (Figure 4). What seems more of a problem is the accentuated plateauing at the tip of the particles. The stair-case aspect (see Figure 3) is due to the integer value of disparity from

which depth is evaluated. A 1.0-mm vertical accuracy does not give as much resources to accurately plot small grains vertical shape as would allow 0.5-mm accuracy. The comparison of the PDFs (Figure 5) shows that there is little difference in the gravel-bed elevations as measured with setup 1 and setup 6. The Z_{MAX} value is slightly increased with setup 6, maybe because the vertical accuracy is too large to accurately locate the tip of the grains and this tends to make an overestimate of the highest peak. Otherwise, the extracted metrics correspond well with those obtained with setup 1 (Table 4).

Table 4 Summary of the metrics extracted from the detrended DEMs restricted to 450 x 400-mm. Only the values obtained with setup 1 are presented, the others are expressed as a percentage of these values.

	Setup 1	**Setup 2**	**Setup 3**	**Setup 4**	**Setup 5**	**Setup 6**
Z_{MIN} (mm)	**-11.06**	241 %	96 %	94 %	82 %	97.5 %
Z_{MAX} (mm)	**+11.69**	148.5 %	105.5 %	134.5 %	158.5 %	112.5 %
ΔZ (mm)	**22.76**	193.5 %	101 %	115 %	121.5 %	105 %
σ_Z (mm)	**3.06**	74.5 %	99 %	100 %	96.5 %	103 %

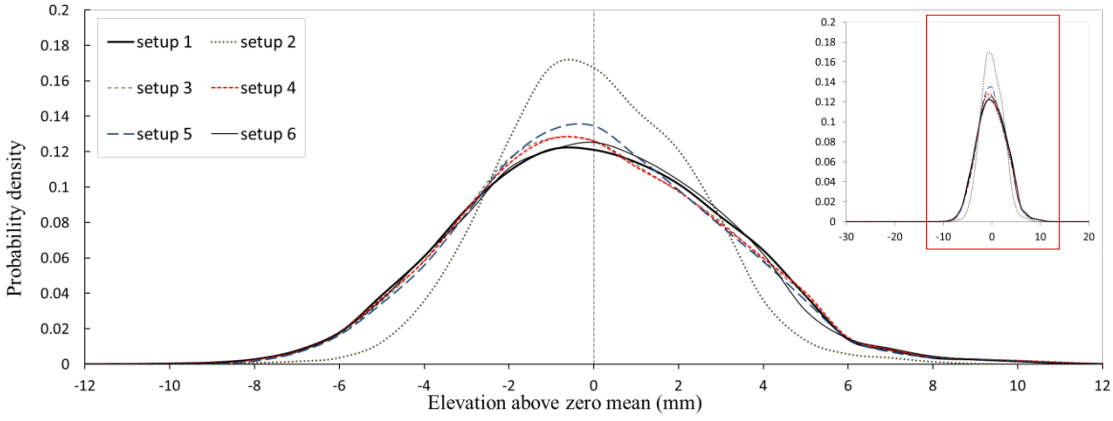

Figure 5 Probability Distribution Functions (PDFs) of bed surface elevations over the small measurement window, zoomed on the red-squared zone of interest.

5 DISCUSSIONS

Compared to previous close-range photogrammetric measurements of gravel-beds, where a self-calibration technique is utilized in addition to ground control points and total stations to determine the exterior orientation (Butler et al., 2002), a simplified yet accurate calibration method was employed in our work. When done in-situ, this calibration enables the refraction correction to be automatically accounted in the calibration parameters (Bruno et al., 2011). The small values of the rectification error observed in our test after through-water calibration of setups 3, 4 and 5 (Table 4) confirm that Zhang calibration is suitable for two-media photogrammetry.

In practice, the acquisition of images of the checkerboard placed underwater was not without difficulties. A long interval (40-s) between two images was necessary to ensure free surface waves were sufficiently small and good photographs were obtained through-water. Previous two-media photogrammetric studies used a Perspex skimmer device to flatten the water surface (Butler et al., 2002, Rapp et al., 2012) and take photographs through the Perspex sheet. It is supposed that calibration data can be obtained beneath the skimmer with little change to the presented method.

In the case of 40-mm water depth, the refraction correction was not accounted because of in-air calibration. This resulted in the DEM with the biggest error rate. Errors were located near the DEM's edges, where the effect of refraction is accentuated, with the center of the DEM presenting good results. This shows that in-air calibration enables to reconstruct submerged scenes, as long as the effect of refraction of optical rays is weak, i.e. when the measurement window (and the water depth) is small.

Even with a thorough in-situ calibration, water depth inexorably tends to deteriorate photogrammetric data. Larger rectification errors and RSEV were obtained with through-water

photogrammetry (Table 2 and Table 3). This in turn results in accentuated chance of mismatched pixels and larger occurrence of errors in the DEMs. However, with water depths smaller than 200-mm, through-water measurement is very similar to in-air.

To date, most photogrammetric measurements have been done on exposed gravel-beds. In the laboratory, this required the experiment to be halted and the flume drained. Refilling the flume to continue the experiment may create changes on the grains' arrangement at the bed surface (Bouratsis et al., 2013). In light of our results, the presented method for two-media photogrammetry should enable to run complete experiments, without halts to undertake measurements, in future. Nevertheless, depending on the experimental flow rate and water depth, it might be necessary to adjust the water depth to a suitable value (preferably less than 200-mm for the present scenario) and reduce the flow rate before measurement. This will not create any change on the gravel-bed surface, at least if the process of reducing/re-increasing the flow rate/water depth is done slowly.

The possibility of large surface coverage, without increasing the measuring time, is clearly an advantage of stereo-photogrammetry, especially when compared with 'active techniques', where measurement is done point-by-point. In our test, the 850 x 400-mm DEM raised the issue of accentuated plateauing at the tip of the particles because of a large vertical accuracy. The horizontal measurement spacing was however still adequate to differentiate sediment particles lying at the gravel-bed surface. In the field, where sediment mixtures are generally coarser than in the laboratory, a 1-mm vertical accuracy should not be a problem. But in the laboratory, the survey of large test sections would best be executed by merging several DEMs of smaller size, as it was done in Chandler et al. (2001), or by employing very high-resolution cameras now becoming available.

Finally, no data post-processing (except point clouds' transfer to DEMs) was used in this study to show the overall capabilities of photogrammetric means to measure fine gravel sediment in the laboratory. Decimating the number of points during point cloud to DEM transfer will smooth the data, similarly to interpolating initial data on a coarse grid. In Hodge et al. (2008), a RSEV filter helped improve original laser-scanned DEMs. In our study, very small RSEV suggest that RSEV filters will have very little effect on DEM quality. Other filters must thus be envisaged for photogrammetric data.

6 CONCLUSIONS

This study has presented the use of high-resolution consumer-grade cameras and non-commercial photogrammetric software in hydraulic experiments measuring the morphology of gravel-beds at the grain-scale. The chosen calibration technique differs from previous applications of stereo-photogrammetry in hydraulic engineering and obviated the need to glue photo-controlled targets on the gravel-bed surface and measure their elevations with additional instruments. The employed calibration method, when done in-situ, will enable to directly account for the refraction of the light rays at the air-water interface, yet some practical difficulties are discussed.

Different measurement scenarios were used to answer the experimental requirements and provide the best measurement specifications. The results show that stereo-photogrammetry is able to measure through-water submerged topographies, with small water depth, without losing accuracy. For instance, data obtained with water depths of 100-mm and 150-mm were statistically very similar to those obtained in air.

Means to undertake the internal assessment of the photogrammetric process steps were proposed and focused on the stereo rectification and the stereo matching. It showed that through-water photogrammetry is more difficult than in-air because of deteriorated calibration results and stereo correspondence in images.

Further research is required to test the effect of flow rate on DEM quality, as well as the effect of grid spacing and data smoothing on the metrics extracted from the DEMs.

References

Bertin S., Friedrich H., Chan E. and Delmas P., 2012. The development and internal assessment of a high-resolution, non-proprietary, stereo-photogrammetric setup for hydraulic experiments. Proceedings of the 27th Conference on Image and Vision Computing New Zealand. Dunedin, New Zealand, ACM**:** 515-520.

Bertin S., Friedrich H. and Heays K., 2011. Evaluating the use of stereo-photogrammetry for gravel-bed roughness analysis. Proceedings of the 26th Conference on Image and Vision Computing New Zealand. Auckland, New Zealand**:** 41-46.

Bouratsis P., Diplas P., Dancey C. L. and Apsilidis N., 2013. High-resolution 3-D monitoring of evolving sediment beds. Water Resources Research, 49(2), 977-992.

Bruno F., Bianco G., Muzzupappa M., Barone S. and Razionale A. V., 2011. Experimentation of structured light and stereo vision for underwater 3D reconstruction. ISPRS Journal of Photogrammetry and Remote Sensing, 66(4), 508-518.

Butler J. B., Lane S. N. and Chandler J. H., 2001. Characterization of the structure of river-bed gravels using two-dimensional fractal analysis. Mathematical Geology, 33(3), 301-330.

Butler J. B., Lane S. N., Chandler J. H. and Porfiri E., 2002. Through-Water Close Range Digital Photogrammetry in Flume and Field Environments. The Photogrammetric Record, 17(99), 419-439.

Chan Y. H., Nguyen M., Gastelum A., Yang S., Gong R., Liu N., Delmas P., Gimel'farb G., Bertin S. and Friedrich H., 2012. The Ngongotaha river UDPS experiment: low-cost underwater dynamic stereo photogrammetry. Proceedings of the 27th Conference on Image and Vision Computing New Zealand. Dunedin, New Zealand, ACM**:** 412-417.

Chandler J., Shiono K., Rameshwaran P. and Lane S., 2001. Measuring Flume Surfaces For Hydraulics Research Using a Kodak DCS460. The Photogrammetric Record, 17(97), 39-61.

Fusiello A., Trucco E. and Verri A., 2000. A compact algorithm for rectification of stereo pairs. Machine Vision and Applications, 12(1), 16-22.

Gimel'farb G., 2002. Probabilistic regularisation and symmetry in binocular dynamic programming stereo. Pattern Recognition Letters, 23(4), 431-442.

Goring D. G., Nikora V. I. and McEwan I. K., 1999. Analysis of the texture of gravel-beds using 2-D structure functions. Proceedings of the I.A.H.R. Symposium on River, Coastal and Esturine Morphodynamics, Genova, Italy**:** 111-120.

Hodge R., Brasington J. and Richards K., 2008. In situ characterization of grain-scale fluvial morphology using Terrestrial Laser Scanning. Earth Surface Processes and Landforms, 34(7), 954-968.

Mao L., Cooper J. R. and Frostick L. E., 2011. Grain size and topographical differences between static and mobile armour layers. Earth Surface Processes and Landforms, 36(10), 1321-1334.

Nikora V. I., Goring D. G. and Biggs B. J. F., 1998. On gravel-bed roughness characterization. Water Resources Research, 34(3), 517-527.

Rapp C., Eder K. and Stilla U., 2012. 3D determination of the evolution of a scour hole by photogrammetric means. Proceedings of the River Flow 2012, San Jose, Costa Rica, Taylor & Francis Group**:** 943-950.

Smart G., Aberle J., Duncan M. and Walsh J., 2004. Measurement and analysis of alluvial bed roughness. Journal of Hydraulic Research, 42(3), 227-237.

Smith M., Vericat D. and Gibbins C., 2012. Through-water terrestrial laser scanning of gravel beds at the patch scale. Earth Surface Processes and Landforms, 37(4), 411-421.

USNCTAM, 2006. Research in Fluid Mechanics: Meeting National Needs.U.S. National Committee on Theoretical and Applied Mechanics (USNCTAM).

Westaway R. M., Lane S. N. and Hicks D. M., 2001. Remote Sensing Of Clear-Water, Shallow, Gravel-Bed Rivers Using Digital Photogrammetry. Photogrammetric Engineering & Remote Sensing, 67(11), 1271-1281.

Zhang Z., 1998. A Flexible New Technique for Camera Calibration. IEEE Transactions on Pattern Analysis and Machine Intelligence, 22(11), 1330-1334,2000.